# **Inorganic Chemistry**

pubs.acs.org/IC Article

# Synthesis and Conformational Dynamics of Selenanthrene (Oxides): Establishing an Energetic Flexibility Index for Scaffolds

Alec T. Larson, Brett Boyle, Jordan Labrecque, Anh Ly, Cecilia Bui, Serhii Vasylevskyi, and Michael J. Rose\*



Cite This: Inorg. Chem. 2024, 63, 10240-10250



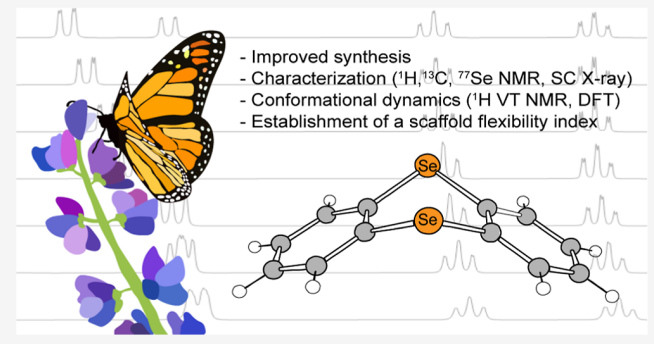
**ACCESS** 

III Metrics & More

Article Recommendations

s Supporting Information

**ABSTRACT:** The use of new dynamic scaffolds for constructing inorganic and organometallic complexes with enhanced reactivities is an important new research direction. Toward this fundamental aim, an improved synthesis of the dynamic scaffold selenanthrene, along with its monoxide, *trans*-dioxide and the previously unknown trioxide, is reported. A discussion of the potential reaction mechanism for selenanthrene is provided, and all products were characterized using <sup>1</sup>H, <sup>13</sup>C, and <sup>77</sup>Se nuclear magnetic resonance (NMR) spectroscopy and single-crystal X-ray crystallography. The dynamic ring inversion processes (i.e., "butterfly motion") for selenanthrene and its oxides were investigated using variable-temperature <sup>1</sup>H NMR and density functional theory calculations. The findings suggest that selenanthrene possesses a roughly equal



barrier to inversion as its sulfur analogue, thianthrene. However, selenanthrene oxides evidently possess larger inversion barriers as compared to their sulfur analogues due to the enhanced electrostatic intramolecular interactions inherent between the highly polar selenium—oxygen bond and adjacent C–H moieties. Finally, we propose a quantitative "flexibility index" in deg/(kcal/mol) for various tricyclic scaffolds to provide researchers with a comparative scale of dynamic motion across many different systems.

## 1. INTRODUCTION

The preparation of selenanthrene (1) was first reported over 125 years ago, but it has received relatively little attention outside of academic research. However, a recent publication demonstrated that 1 undergoes pressure-induced roomtemperature phosphorescence enhancement, underscoring a potential new use of a long-known chemical. This effect was ultimately attributed to a mechanism that involves foldinginduced spin-orbit coupling enhancement, a phenomenon made possible by the conformational mobility of 1 (Scheme 1). On the other hand, the homologous sulfur-analogue, thianthrene and in particular thianthrene-5-oxide has received substantially more attention due to its use as a mechanistic probe for determining the electrophilic or nucleophilic character of oxidants.<sup>3,4</sup> In addition, thianthrene and its oxides have been investigated from both theoretical<sup>5,6</sup> and experperspectives regarding their conformational mobi-

Scheme 1. Conformational Equilibrium and Planar Transition State of Thianthrene

lity. In solution, both thianthrene and 1 and their S/Se-oxides exist in conformational equilibria. They fold (or "flap") about the axis that bisects the two chalcogen atoms and can rapidly interconvert via a ring inversion process (Scheme 1a). For ring inversion to occur, the ring must pass through a planar transition state (Scheme 1b).

A recent publication from our group investigated the role that distal scaffold flexibility plays in accelerating the rate of ligand substitution kinetics in manganese(I) tricarbonyls. <sup>10</sup> In that case, a bis-pyridine ligand constructed upon a flexible thianthrene scaffold afforded enhanced ligand substitution rates as compared to an analogous ligand using a rigid anthracene scaffold. <sup>10</sup> In connection with this work, 1 is now under consideration as a ligand scaffold candidate due to its presumed conformational mobility. It was, however, not readily apparent from the available literature whether 1 was more or less conformationally dynamic than its lighter-atom analogue, thianthrene. To elucidate this point, herein, we report an

Received: February 15, 2024 Revised: April 17, 2024 Accepted: April 17, 2024 Published: May 17, 2024





Scheme 2. (a) Erroneous Structure Assignment for the Conditions Previously Reported<sup>12</sup> for 1; (b) Patented Conditions<sup>13</sup> for the Synthesis of Thianthrene; (c) Single-Crystal X-ray Structure of 1,2-Bis(4-bromophenyl)diselane Determined in This Work Resulting from Conditions in (a)<sup>a</sup>

"(i) trifluoroacetic acid (0.5 equiv), potassium persulfate (1 equiv), benzonitrile (5 equiv), room temperature, 3 h.

improved synthesis of **1** and its oxides. Products were characterized by <sup>1</sup>H NMR, <sup>13</sup>C NMR, <sup>77</sup>Se NMR and X-ray crystallography. The conformational dynamics of each molecule were investigated using variable-temperature nuclear magnetic resonance (NMR) spectroscopy and density functional theory (DFT) calculations, and ultimately, we provide a new quantitative metric of dynamic motion, namely, the energetic flexibility index, that expresses the extent of flexibility of scaffolds in units of deg/(kcal/mol).

## 2. RESULTS AND DISCUSSION

2.1. Synthesis and Discussion of the Potential Mechanism for Selenanthrene Formation. Several synthetic procedures that furnish 1 have been reported over the years. Most suffer from poor yields, forcing conditions, and the use of toxic selenium reagents or altogether inaccurate products. A comprehensive review of synthetic methods for 1,4-diselenins has been previously published. 11 In fact, one article12 reported a procedure for 1; however, their spectroscopic characterization is inconsistent with 1. We independently tested their reported reaction conditions and found that the product was not 1 but instead the diselenide compound 1,2-bis(4-bromophenyl)diselane (Scheme 2a,c). We unambiguously characterized this "incorrect" product by <sup>1</sup>H NMR, <sup>13</sup>C NMR, <sup>77</sup>Se NMR and X-ray crystallography; moreover, these data were consistent with their reported characterization, confirming the inaccurate identity previously assigned to this structure. See the Supporting Information for the full characterization of 1,2-bis(4-bromophenyl)diselane.

Coincidentally, a database search returned a patented method for a synthesis of *thianthrene*, which employed inexpensive reagents and relatively mild conditions (Scheme 2b). <sup>13</sup> Intrigued, we applied a procedure similar to that for the synthesis of 1. In this way, 1 was indeed obtained, albeit initially in a low yield (30%). Several optimization experiments were performed to improve the yield of the reaction by altering the copper salt, base selection, equivalents of selenium, temperature, and reaction time (Table 1). See the Experimental Section for the general procedure used for the optimization experiments.

Initial replication of the reported conditions in the patent was performed by substituting elemental selenium in place of

Table 1. Selenanthrene Optimization Experiments<sup>a</sup>

entry	cat	base	equiv Se	temp (°C)	time (h)	% conv
1	CuBr	$K_2CO_3$	1	90	16	30
2	CuBr	$K_2CO_3$	1	140	16	50
3	CuI	$K_2CO_3$	1	140	16	10
4	$Cu(OAc)_2$	$K_2CO_3$	1	140	16	60
5	$Cu(OAc)_2$	$Cs_2CO_3$	1	140	16	38
6	$Cu(OAc)_2$	$Na_2CO_3$	1.5	140	16	86
7	$Cu(OAc)_2$	$K_2CO_3$	1.5	140	16	83
8	$Cu(OAc)_2$	$Na_2CO_3$	1.5	100	96	77 <sup>b</sup>
9	$Cu(OAc)_2$	$K_2CO_3$	1.5	100	72	87 <sup>b</sup>
10 <sup>c</sup>	$Cu(OAc)_2$	$K_2CO_3$	1	140	16	29
11 <sup>c</sup>	_	$K_2CO_3$	1	140	16	20
$12^d$	$Cu(OAc)_2$	$K_2CO_3$	1.5	100	72	55

"Unless otherwise noted, reactions were performed on the 1 mmol scale relative to 1,2-diiodobenzene at a concentration of 0.5 M. Conversions were determined by <sup>1</sup>H NMR. <sup>b</sup>Isolated yield, >10 mmol scale. <sup>c</sup>Reaction performed without addition of 1,10-phenanthroline. <sup>d</sup>Reaction performed with inclusion of 25 mol % triphenylphosphine.

sulfur (S<sub>8</sub>) which provided a conversion of 30% (Table 1, entry 1). Increasing the reaction temperature from 90 to 140 °C substantially improved conversions. Next, several copper precatalysts were screened (Table 1, entries 2–4). Copper(II) acetate outperformed other copper salts and was thus used for the remainder of the screening. Several bases were also screened, with sodium carbonate and potassium carbonate performing equally; cesium carbonate, on the other hand, had a deleterious effect (Table 1, entry 5). Increasing the equivalents of elemental selenium from 1 to 1.5 provided good improvements in conversion (Table 1, entries 6 and 7). Conversely, heating for several days at 140 °C resulted in tarry solutions caused by decomposition of both the starting 1,2diiodobenzene and 1. To address this, reaction temperatures were lowered to 100 °C and reaction times extended to several days (Table 1, entries 8 and 9). This mitigated tar formation and provided very good isolated yields, even on scales >10

mmol. In this case, potassium carbonate provided better results than sodium carbonate. Conditions were screened that omitted the ligand (Table 1, entry 10) and that omitted both a copper salt and ligand (Table 1, entry 11). Surprisingly, both sets of conditions gave some conversion to 1, albeit in a poor yield. This demonstrated that the process could occur uncatalyzed, perhaps an indication of the potent nucleophilicity of selenides. In an attempt to shorten reaction times, 25 mol % triphenylphosphine was included as a phase-transfer catalyst (Table 1, entry 12); this unfortunately provided lower conversion than the standard conditions (entry 9); presumably the phosphine deactivates catalytically relevant species. Concomitant with our work, an article detailing the synthesis of a pair of isomeric selenanthrene-bridged molecular cages was published that utilizes analogous reaction conditions (DMA, K<sub>2</sub>CO<sub>3</sub>, 150 °C, 72 h). <sup>14</sup> This lends credence to the generality of the copper-catalyzed approach for preparing organoselenium compounds from aryl iodides and elemental selenium.

A possible mechanism for a general chalcogenation/diaryl selenide coupling reaction employing a Cu<sup>I</sup>/"Cu<sup>III</sup>" cycle is presented in Scheme 3. [Note: in accordance with the work of

Scheme 3. Proposed Mechanism for a General Chalcogenation/Diaryl Selenide Coupling Reaction<sup>a</sup>

3 Se + 3 
$$K_2CO_3$$
  $\longrightarrow$   $2K_2Se + K_2SeO_3 + 3CO_2$ 

$$[Cu^I(phen)X]_2$$
ArSeAr
$$Cu^I(phen)X$$

$$Ar - Cu^{II} - phen^+$$
SeK D  $X$ 

$$Ar - Cu^{II} - phen^+$$

$$C$$

$$K_1$$

$$K_2Se$$
ArSeK

"X in this case denotes a general counteranion, either acetate or iodide. The abbreviation phen refers to 1,10-phenanthroline.

Lancaster et al., 15 we have opted to depict all "Cu<sup>III</sup>" species as instead existing as Cu<sup>II</sup>, with the additional oxidation equivalent present on the ligand; thus 1,10-phenanthroline is depicted as a radical cation species.] The reduction of elemental selenium to a nucleophilic selenide salt is likely required before subsequent reaction steps can occur. 16 It is long-known that elemental sulfur will disproportionate under basic conditions, yielding a mixture of sulfides and sulfites.<sup>1</sup> The disproportionation of elemental selenium into a mixture of selenides and selenites is known to occur in the presence of aqueous alkali, although a mixture of polyselenides is typically obtained. 18 It is conceivable that a similar disproportionation mechanism occurs in the presence of alkali carbonates such as the one shown in Scheme 3. We attempted to characterize the selenide species formed in situ under the optimized reaction conditions, although we were unable to observe any resonances by <sup>77</sup>Se NMR (see the Supporting Information for details). Dimer A has been previously observed to be a resting state in the catalytic cycle for the synthesis of diaryl selenides. " Presumably, dimer A must split into monomer B before it can enter the catalytic cycle. The equilibrium between A and B is

likely dependent on the iodide (or other halide) concentration, which might explain why  $Cu(OAc)_2$  is a superior precatalyst as it would limit the formation of dimer **A** by minimizing the iodide concentration.

Oxidative addition of aryl iodide to B would yield intermediate C, which has dual purposes in this proposed mechanism. On the one hand, it can assist the chalcogenation of aryl iodides by undergoing transmetalation with potassium selenide to yield intermediate D, which could then undergo reductive elimination to produce aryl selenolate and monomer B. A similar series of steps was proposed as the mechanism for a copper-catalyzed diaryl sulfide synthesis. 16 On the other hand, if intermediate C instead transmetalates with the aryl selenolate, intermediate E is obtained, which has been previously proposed. 19 Reductive elimination of E yields diaryl selenide and monomeric species B. For 1, a subsequent series of chalcogenation and aryl selenolate/aryl iodide coupling steps is required, but it is conceivable that the latter could occur intramolecularly due to the close proximity of the selenolate and aryl iodide.

Synthesis of selenanthrene-5-oxide (2) was previously accomplished using m-CPBA in DCM solution, which was successfully reproduced herein. Driving the further oxygenation of 2 to selenanthrene-5,10-dioxide (3) has been accomplished by several unconventional strategies, such as oxidation of 1 with nitric acid<sup>1,21</sup> and the hydrolysis of selenanthrene tetrachloride. As such, to achieve more straightforward and uniform synthetic procedures, we attempted to simply extend the use of m-CPBA under more forcing (but still mild) conditions to dioxides 3 and trioxide 4 (Scheme 4).

Scheme 4. Synthetic Scheme for 1-5<sup>a</sup>

"(i) m-CPBA, 0 °C, 2 h, DCM; (ii) 3 equiv m-CPBA, reflux, 16 h, DCM; (iii) 4 equiv m-CPBA, reflux, 48 h, DCM; (iv) 10 equiv m-CPBA, reflux, 72 h, 1,2-dichloroethane.

Indeed, we found *m*-CPBA to be a quite versatile reagent for the synthesis of the oxides of **1**. A slight excess of *m*-CPBA while maintaining the reaction at 0 °C resulted in the selective formation of **2**. However, 3 equiv of *m*-CPBA in conjunction with refluxing for 16 h cleanly provided trans-3. The cis-3 isomer was not isolated, but it was observed to form in situ via the isomerization of trans-3 by <sup>1</sup>H NMR at ambient temperatures. This is consistent with the observation that

selenoxides are known to undergo racemization if moisture is not carefully excluded from the reaction.<sup>23</sup> Previous reports included neither 4 or selenanthrene-5,5,10,10-tetroxide (5) (both containing a selenone moiety). 1,21,22 However, we found that 4 did form after treating 1 with 4 equiv of m-CPBA and heating for 48 h. We made a minor attempt to obtain 5 by reaction of 1 with 10 equiv of m-CPBA in refluxing 1,2dichloroethane for 72 h. The major product from this reaction remained as 4; however, a very downfield <sup>1</sup>H NMR resonance was observed at 8.84 ppm, which we attribute to the presence of 5; we postulate that 5 could be obtained more cleanly if a stronger oxidant was used. One such reagent is dioxirane; it is more nucleophilic than m-CPBA and thus would more easily oxidize the electrophilic selenoxide in 4.24

2.2. Single-Crystal X-ray Crystallographic Studies. Notably, the first crystallographic study of 1 was performed in 1942, and while the study did not determine a complete structure, the authors attempted to estimate the dihedral angle between the phenyl rings of 1.25 In 1988, a full structure of 1 was published, but it was only refined isotropically. <sup>26</sup> Only very recently, a full anisotropically refined structure of 1 was published.<sup>2</sup> To the best of our knowledge, there are no previously reported X-ray crystal structures of oxides of 1. To this end, structural characterization of 1, 2, trans-3 and 4 was performed in parallel using single-crystal X-ray crystallography. Full crystallographic details are provided in the Supporting Information. Figure 1 illustrates selected bonding metrics for 1, 2, trans-3 and 4.

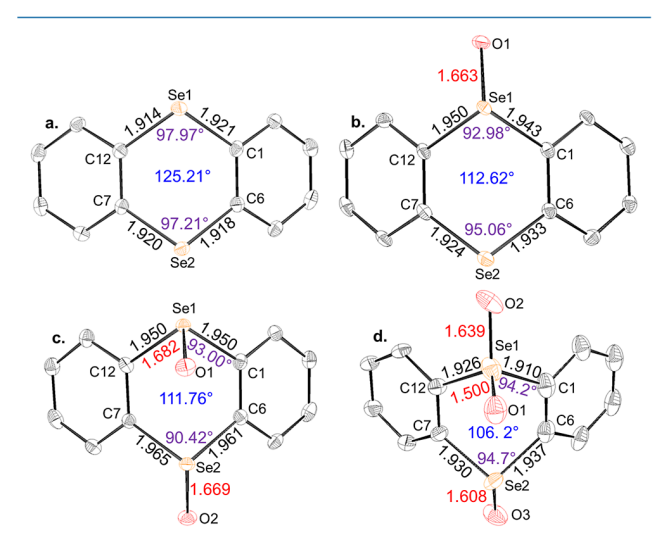


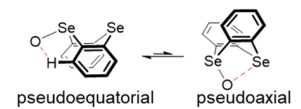
Figure 1. ORTEP diagrams (50% thermal ellipsoids) resulting from the X-ray crystal structures of (a) 1; (b) 2; (c) trans-3; and (d) 4 along with selected bonding metrics (bond lengths in Å). Se-C and Se-O bond lengths are shown in black and red, respectively; C-Se-C bond angles are shown in violet, and fold angles (defined as the dihedral angle formed between the planes of the aromatic rings) of the scaffolds are shown in blue. H atoms are omitted for clarity. ORTEP diagrams were generated using the Ortep3 software package.27

For diphenyl selenide moieties in 1 and 2, the Se-C bond lengths were roughly 1.92 Å. On the other hand, Se-C bond lengths elongated slightly to about 1.95 Å in the selenoxide moieties in 2 and trans-3. Somewhat counterintuitively, this trend evidently reverses in compound 4. The selenone moiety in 4 has Se-C bond lengths that are comparable to the Se-C bond lengths in 1. A similar trend is observed for the

selenoxide moiety in 4, wherein the Se-C bond lengths of about 1.93 Å are somewhat shortened compared to those in 2 and trans-3. Se-O bond lengths in 2, trans-3 and 4 are quite consistent with each other, all within the range of 1.60-1.68 Å. An exception to this trend occurs in the selenone moiety in compound 4. The pseudoequatorial oxygen (O2 in 4) has a typical Se-O bond length of about 1.64 Å (Scheme 3). Remarkably, the Se-O bond length of the pseudoaxial oxygen (O1 in 4) is just 1.50 Å. This is atypical of selenone moieties in general, which typically display Se-O bond lengths of over 1.60 Å.<sup>28,29</sup>

Upon consideration of the fold angle (defined as the dihedral angle formed between the planes of the aromatic rings), the general trend observed is that the fold angle decreases with an increasing number of oxygen atoms appended to the scaffold. This contrasts with the trend observed with thianthrene and its oxides, wherein the fold angles in the crystal phase vary by only 1 or 2° even upon changing the number of oxygen atoms from 0 to 3.30-32 The reason for this trend is likely the stronger intramolecular electrostatic interaction between the pseudoequatorial selenoxide moiety and the peri hydrogen atoms on the scaffold (Scheme 5). This is a stabilizing interaction, and presumably

# Scheme 5. Equilibrium of Pseudoequatorial and Pseudoaxial Conformers of 2<sup>a</sup>



<sup>a</sup>The pseudoequatorial conformer shows the interaction between the selenoxide moiety and the peri hydrogen atoms. The pseudoaxial conformer shows the transannular interaction between the selenoxide moiety and the adjacent selenide moiety. Analogous interactions also exist in trans-3 and 4.

the scaffold bends to facilitate this. This interaction is present in all of the oxygen-containing scaffolds, namely, 2, trans-3 and 4. These data suggest that adding a pseudoequatorial selenoxide moiety to the scaffold produces a dramatic change in fold angle. For example, 1 has a fold angle of 125.2°, but contracts by nearly 13° when a pseudoequatorial selenoxide moiety is added: 2 possesses a fold angle of 112.6°. On the other hand, when the scaffold is further oxidized to trans-3, the fold angle contracts by less than 1°. This is likely due to the second selenoxide moiety adopting a pseudoaxial position, which lacks the electrostatic interaction with the peri hydrogen atoms. The fold angle contracts further in 4 to 106.2° as it contains two such electrostatic interactions between the pseudoequatorial selenoxide moiety and the peri hydrogen atoms, one on the selenoxide (O2) moiety and one on the selenone (O3) moiety.

There appears to be a rough correlation between the fold angle and C-Se-C bond angles; that is, as the fold angle becomes more acute, so do the C-Se-C bond angles in the scaffold. This is geometrically obligatory, but the other factor is evidently the oxidation state of selenium. Even though the fold angle is quite contracted in 2, the C-Se-C bond angle of the selenide moiety is still about 95.0°. This is reasonably close to the C-Se-C bond angles seen in 1, which are about 97-98°. On the other hand, the C-Se-C bond angles in selenoxide

and selenone moieties are generally more acute, ranging from 90.4 to  $94.7^{\circ}$  in compounds 2, trans-3 and 4.

**2.3. Variable Temperature** <sup>1</sup>H NMR. To investigate the conformational dynamics of 1 and its oxides, we utilized variable temperature <sup>1</sup>H NMR spectroscopy. In principle, 1 should not display coalescence because it cannot undergo a change in its "nuclear spin system" (referred to hereafter simply as "spin system") as it changes from being conformationally dynamic to conformationally locked on the NMR time scale. If 1 is presumed to be conformationally dynamic, it possesses  $D_{2h}$  symmetry, and thus the protons at ring positions 1 and 4 related by both mirror plane and rotational symmetry, and the same is true of protons at ring positions 2 and 3 (Figure 2). If 1 is presumed to be conformationally locked, it

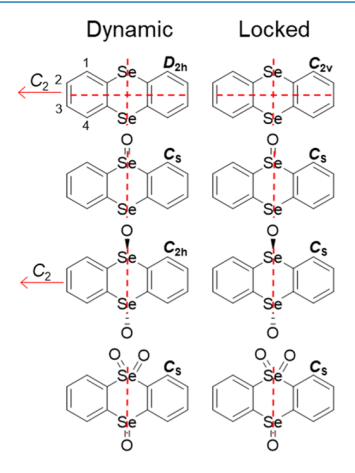


**Figure 2.** Symmetry elements and point group (bolded) for conformationally dynamic and locked conformers of 1, 2, trans-3 and 4. Mirror planes are indicated by dashed red lines;  $C_2$  rotational axes are indicated with red arrows. Ring numbering scheme is shown on the top-left molecule.

possesses a  $C_{2v}$  symmetry. The rotational symmetry is lost, but the protons at ring positions 1 and 4 are still related by mirror symmetry, as are the protons at positions 2 and 3. Thus, in both cases, protons at positions 1 and 4 will be chemically equivalent but magnetically inequivalent; the same is true of protons at positions 2 and 3.

As such, 1 is not capable of undergoing a change in the spin system, and thus broadening and coalescence of peaks are not expected. Indeed, solutions of 1 in CD<sub>2</sub>Cl<sub>2</sub> displayed sharp resonances from +20 to -80 °C, with no evidence of coalescence (Figure S11). The observed AA'XX' spin-system is characteristic of ortho-disubstituted aromatic molecules.<sup>33</sup> Selenanthrene-5-oxide was also investigated in CD<sub>2</sub>Cl<sub>2</sub> solution from +20 to -95 °C (Figure 3) and in DMSO- $d_6$ solution from +20 to +100 °C (Figure 4). Again, no coalescence of the resonances was observed. This is expected because 2 cannot undergo a change in the spin-system. Regardless of whether 2 is presumed to be conformationally dynamic or conformationally locked, the molecule will possess a  $C_S$  symmetry, and the protons at ring positions 1, 2, 3 and 4 will be chemically inequivalent (Figure 2). Interestingly, 2 displayed a drastic upfield temperature-dependence for the proton resonances of the hydrogen atoms peri to the selenoxide moiety (Scheme 5). A similar phenomenon was observed in a previous study of thianthrene 5-oxide; this phenomenon was interpreted as a combination of shielding

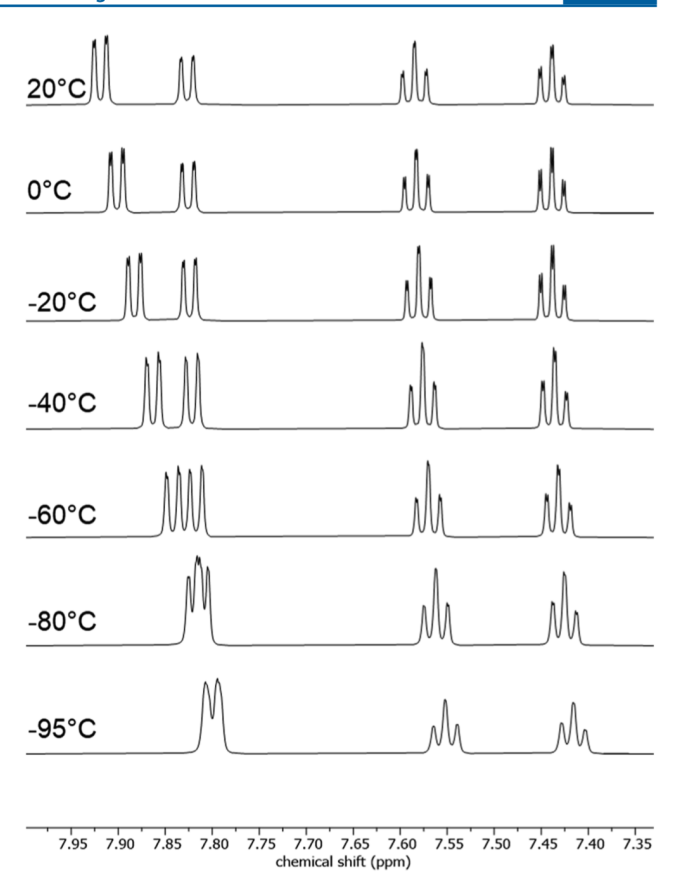


Figure 3. Variable temperature <sup>1</sup>H NMR (600 MHz) of 2 in CD<sub>2</sub>Cl<sub>2</sub>.

effects related to changes in solvation and anisotropy of the solvent in addition to the shift of the conformational equilibrium of thianthrene 5-oxide toward the pseudoaxial conformer with decrease in temperature.<sup>7</sup>

In contrast to 1 and 2, trans-3 is capable of undergoing coalescence. If trans-3 is assumed to be conformationally dynamic on the NMR time-scale, its point group is  $C_{2h}$ ; as such, the protons at ring positions 1 and 4 are rendered chemically equivalent because they are related by a  $C_2$ rotational axis, as are the protons at positions 2 and 3. On the other hand, if trans-3 is conformationally locked on the NMR time-scale, its point group is instead  $C_S$  (Figure 2). This descent in symmetry removes the  $C_2$  axis, and as such, protons at positions 1, 2, 3, and 4 are rendered chemically inequivalent. As such, trans-3 should undergo a change in the spin system with a corresponding change in temperature. Indeed, this was observed in the VT <sup>1</sup>H NMR spectra collected in CDCl<sub>3</sub> (Figure 5). While not fully resolved at +55 °C, an AA'XX' spin-system was observed, suggesting that ring inversion is rapid on the NMR time scale. In contrast, at -60 °C, a first order system is observed, indicating that ring inversion is slow on the NMR time scale. The two doublets in the spectrum are separated by 198 Hz at −60 °C.

Due to this large separation, broadening and coalescence of the peaks occur over a wide temperature range, rendering assignment of the coalescence temperature relatively straightforward. The best choice for coalescence occurs at  $-5\pm3\,^{\circ}\mathrm{C}$ , which has an associated inversion barrier of  $\Delta G^{\ddagger}=12.4\pm0.2$  kcal/mol. This is in contrast to *trans*-thianthrene 5,10-dioxide (the corresponding sulfur-analogue of trans-3), which has a ring inversion barrier predicted and measured to be in the

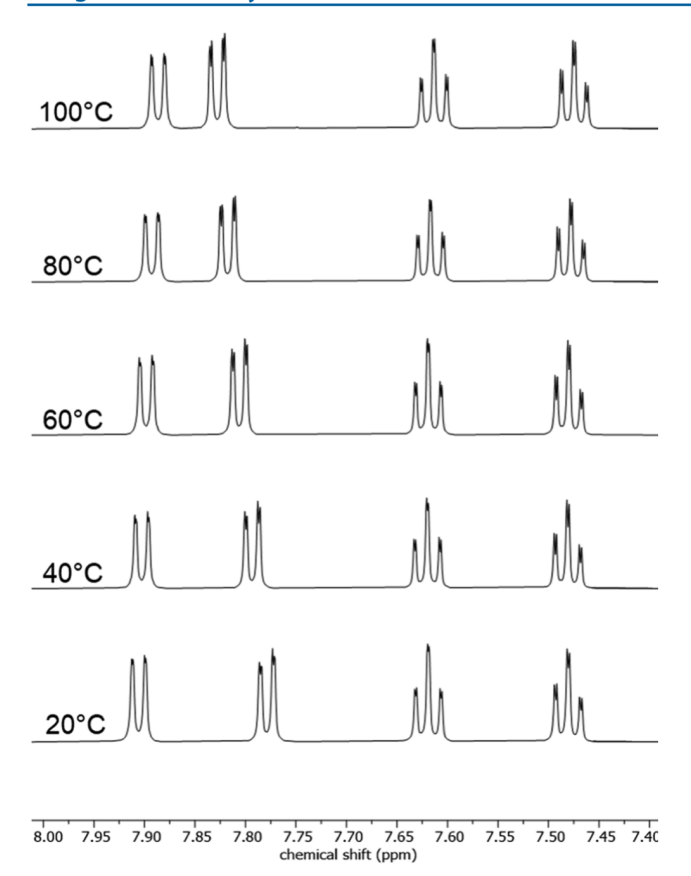


Figure 4. Variable temperature  $^{1}{\rm H}$  NMR (600 MHz) of 2 in DMSO-  $d_{6^{\circ}}$ 

range of 9-10 kcal/mol. The increase in the inversion barrier is probably due to two factors: first, the most important influence is likely the enhanced electrostatic interaction between the peri hydrogen atoms and the selenoxide moiety (Scheme 5) that must be overcome, as compared with the analogous weaker interaction in trans-thianthrene 5,10-dioxide. The Se-O bond has significantly more ionic character relative to an S-O bond; as such, the oxygen in a selenoxide moiety is more negatively charged than in a sulfoxide moiety; the increased electron density at the oxygen atom in the selenoxide moiety increases the strength of the electrostatic interaction with the peri hydrogen atoms. The second (and probably less influential) effect is due to increased bond angle strain in the transition state from the C-Se-C moieties. In general, C-E-C bond angles (where E is a chalcogen) decrease in the  $C_{12}H_8E_2$  series (E = O, 116°; E = S, 100°; E = Se, 98°; E = Te,  $95^{\circ}$ ). 2,31,34,35 For the heavier the chalcogen atom, the C-E-C bond angle must expand to a greater extent in order to accommodate the planar transition state, and as a result, the inversion barrier increases.

No coalescence was expected in 4 because like 2, it cannot undergo a change in the spin-system: Regardless of whether 4 is conformationally dynamic or locked, it will possesses a  $C_{\rm S}$  symmetry, and the protons on ring positions 1, 2, 3 and 4 will be rendered chemically inequivalent, and a first order system should be observed (Figure 2). Indeed, the variable-temperature  $^{1}{\rm H}$  NMR spectra of 4 collected from +20 to -80  $^{\circ}{\rm C}$  in CD<sub>2</sub>Cl<sub>2</sub> (Figure S15) and from +20 to +110  $^{\circ}{\rm C}$  in DMSO- $d_{\rm G}$  (Figure S16) exhibited no coalescence of resonances, and thus no inversion barrier could be calculated. Interestingly, 4 also

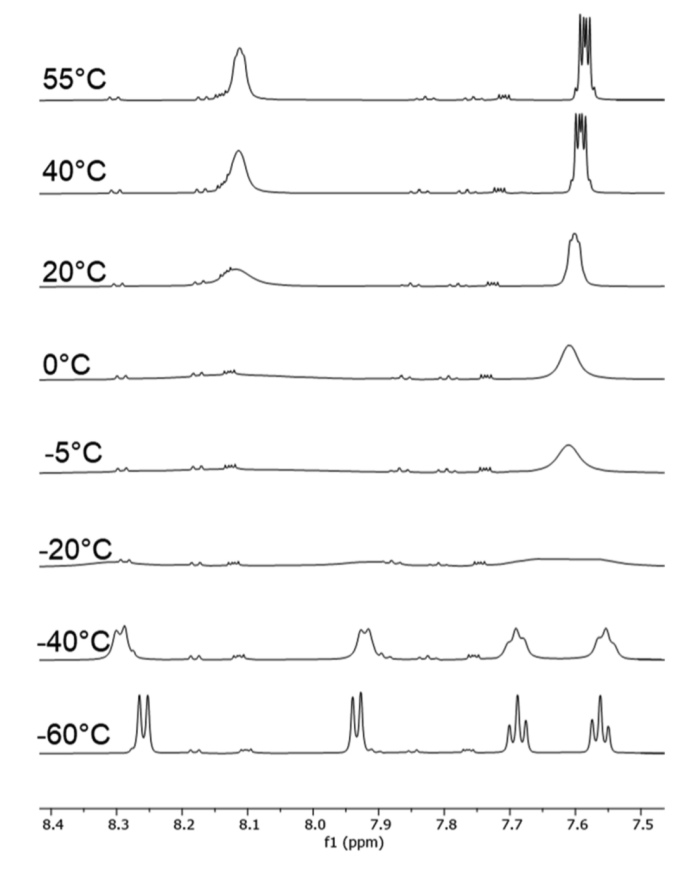


Figure 5. Variable temperature <sup>1</sup>H NMR (600 MHz) of trans-3 in CDCl<sub>3</sub>. A small amount of 2 and cis-3 is present in the spectra.

displays a strong temperature-dependence of the proton resonances peri to the sulfone moiety for similar reasons as discussed previously for 2.

2.4. Ground State, Transition State and Relaxed PES **Calculations.** For technical details regarding calculations, see the Computational Methods section. Highlighting the inherent limited spectroscopic utility of NMR methods in evaluating inversion barriers (due to symmetry properties), the VT NMR analysis provided an inversion barrier only for trans-3. To circumvent this limitation, DFT calculations were employed to predict the inversion barriers of compounds 1-4. Our primary concern was to accurately predict the inversion barriers for 1, 2, trans-3 and 4. This was problematic as we were only able to experimentally determine a ring inversion barrier for trans-3. Nonetheless, we sought a DFT model that accurately predicts  $\Delta G^{\ddagger}$  for trans-3 and would thus serve as a reference to accurately predict the other inversion barriers not accessible by experimental VT-NMR studies. Initial ground state and transition state optimizations were performed at the BP86/ def2-SVP level of theory to interrogate the barrier for ring inversion in 1-4 (Table 2). A full comparison of experimental and computed bonding metrics is beyond the scope of the main text; however, this discussion is duly included in the Supporting Information (in conjunction with Table S7). The computed ring inversion barrier of trans-3 at the BP86/def2-SVP level of theory was 16.7 kcal/mol, in only moderate agreement with the experimental value for trans-3 of  $\Delta G^{\ddagger}$  =  $12.4 \pm 0.2$  kcal/mol. Thus, we sought to improve this by employing a functional and basis set that was better suited to handle selenium containing arenes. To this end, ground state

Table 2. Computed Relative Energies (kcal/mol) of Ground States and Transition States of 1-4

	i <sup>a</sup>	$E_{\mathrm{rel}}^{b}$	$E_{\mathrm{rel}}^{c}$	$E_{\mathrm{rel}}^{}}}}}}$
1 (gs)	0	0.0	0.0	0.0
1 (ts)	1	6.27	6.46	5.99
<b>2</b> (gs)	0	0.0	0.0	0.0
2 (ts)	1	12.17	11.25	8.59
trans-3 (gs)	0	0.0	0.0	0.0
trans-3 (ts)	1	16.70	15.91	13.25
<b>4</b> (gs)	0	0.0	0.0	0.0
<b>4</b> (ts)	1	16.27	14.12	9.54

<sup>a</sup>i refers to the calculated number of imaginary frequency modes. <sup>b</sup>BP86/def2-SVP with no solvation model. <sup>c</sup>OPBE/ZORA-def2-TZVP with no solvation model. dOPBE/ZORA-def2-TZVP with SMD solvation model (chloroform). <sup>e</sup>Note: ground state and transition state structures could not be verified by frequency analysis when including the SMD solvation model (see the Computational Methods section).

and transition state structures of 1-4 were calculated at the OPBE/ZORA-def2-TZVP level of theory, and their relative energies are listed in Table 2. For a discussion of this functional and basis set selection, see the Computational Methods section. Apart from 1, the OPBE/ZORA-def2-TZVP calculations predicted inversion barriers slightly lower than those of the BP86/def2-SVP calculations. Unfortunately, the computed inversion barrier of about 15.9 kcal/mol for trans-3 remained substantially higher than the experimentally determined value of  $\Delta \dot{G}^{\ddagger} = 12.4 \pm 0.2 \text{ kcal/mol.}$ 

Due to the highly ionic nature of selenium-oxygen bonds, we suspected that interaction from the solvent was unaccounted for in the model. Presumably, the solvent interacts with the strongly polarized selenium-oxygen moieties and attenuates somewhat both the electrostatic interaction between (i) the oxygen and the peri hydrogen atoms and (ii) the transannular interaction between the pseudoaxial selenoxide (or selenone) moiety and the adjacent electropositive selenoxide moiety (Scheme 5). To account for solvation, the implicit solvation model, solvation based on density (SMD), was used as implemented in ORCA. Chloroform was selected as the implicit solvent as the experimental measurements for trans-3 were collected in deuterochloroform. Inversion barriers determined from ground state and transition state calculations using OPBE/ZORAdef2-TZVP with implicit SMD solvation (chloroform) are also displayed in Table 2. See the Computational Methods section for an important note about analytical frequency calculations with the SMD solvation model. Beneficially, the computed inversion barrier for trans-3 was 13.3 kcal/mol. While still an overestimate, this value is in much better agreement with the experimentally determined value of  $\Delta G^{\ddagger} = 12.4 \pm 0.2 \text{ kcal/mol}$ for trans-3.

The computed inversion barrier for 1 varied by less than 8% at both levels of theory, even when accounting for solvation. On the other hand, computed inversion barriers for molecules containing polar selenium-oxygen bonds (2, trans-3 and 4) were substantially affected by the inclusion of a solvation model. Comparison of the computed barrier for 4 at the OPBE/ZORA-def2-TZVP level of theory with inclusion of a solvation model decreased the associated inversion barrier by more than 30%. These data suggest that when considering inversion barriers, it is of critical importance to account for solvent interactions of highly polarized moieties.

Lastly, it was deemed meaningful to obtain the potential energy surface (PES) along the "butterfly" motion (i.e., ring inversion) of 1-4. For technical details regarding this procedure, see the Computational Methods section. The PES scan was performed at the OPBE/ZORA-def2-TZVP level of theory with the SMD solvation model using chloroform as the implicit solvent (Figure 6). The points with a relative energy of zero are ground state configurations, while the apex of the curves corresponds to the transition states.

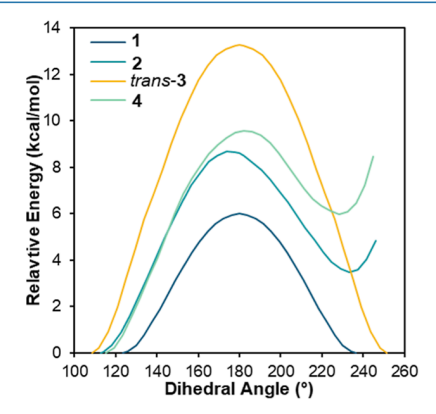


Figure 6. Relaxed PES scan along the "butterfly" motion of 1, 2, trans-3 and 4 at the OPBE/ZORA-def2-TZVP level of theory with the implicit chloroform solvation model.

Both 1 and trans-3 possess symmetric energy profiles as they are geometrically symmetric with respect to ring inversion. On the other hand, 2 and 4 have asymmetric energy profiles, with local minima at a dihedral angle of about 235°. For 2, this local minimum corresponds geometrically to the selenoxide moiety being in a pseudoaxial configuration (Scheme 5). The same is true of 4; however, the local minimum of 4 is destabilized relative to 2, probably due to the mutual clashing interaction between the two pseudoaxial oxygen atoms in this conformation (Scheme 6).

Scheme 6. Conformational Equilibrium of 4, Highlighting the Steric Clashing of Se-O Moieties in Red

While it was not possible to determine equilibrium constants for 2 and 4 from the VT <sup>1</sup>H NMR data, it was now possible to estimate them based on the computed energy differences (OPBE/ZORA-def2-TZVP with chloroform solvation model) between their two conformations. The computed energy differences between the two conformations of 2 and 4 are  $\Delta G$ = 3.47 and 5.98 kcal/mol, respectively. If a temperature of 25 °C is assumed, the corresponding equilibrium constants for 2 and 4 are  $K_{\rm eq} = 2.85 \times 10^{-3}$  and  $4.13 \times 10^{-5}$ , respectively. These values represent equilibria strongly skewed toward the lower energy conformations, suggesting that, in solution, 2 is best thought of as primarily existing in its pseudoequatorial

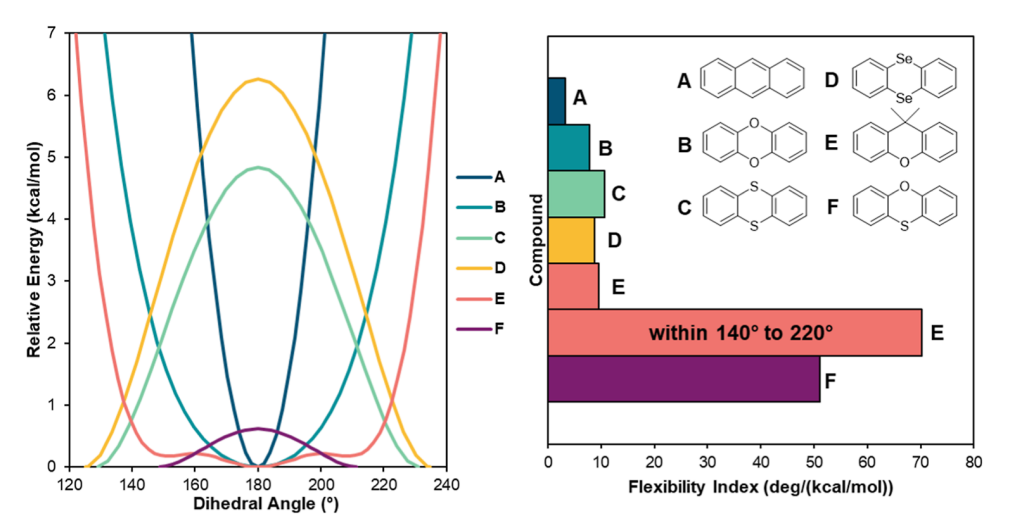


Figure 7. DFT relaxed PES scans (*left*) of the "butterfly" motion of anthracene (A), oxanthrene (B), thianthrene (C), selenanthrene (D), 9,9-dimethylxanthene (E), and phenoxathiin (F) at the BP86/def2-SVP level of theory. The bar chart (*right*) indicates the extent of flexibility per unit energy [i.e., the flexibility index, expressed in units of deg/(kcal/mol)]. To make the most sensible comparisons, the energetic flexibility index for each scaffold was sensibly calculated by either (i) dividing the maximum dihedral angle deviation from 180° allowed within 6 kcal/mol [for (A,B,E)] or (ii) dividing the dihedral angle difference from ground state and transition state configurations by the associated inversion barrier height [for (C,D,F)].

conformer (Scheme 5), while 4 exists chiefly as its mutual pseudoequatorial conformer (Scheme 6).

2.5. Comparison of Relaxed PES Scans of Tricyclic Scaffolds: Energetic Flexibility Index. In connection with ongoing work in our research group regarding flexible tricyclic molecules, <sup>10</sup> we deemed it germane to compare the PES along the "butterfly" motion of 1 against other candidate tricyclic scaffolds. To this end, relaxed PES scan calculations were performed by using DFT at the BP86/def2-SVP level of theory on five other tricyclic molecules (Figure 7). For technical details regarding the calculations, see the Computational Methods section.

To generate a reference point, PES scan calculations were performed on anthracene (Figure 7, scaffold A). Unsurprisingly, deviations from planarity were met with a steep energetic penalty as the scaffold flexes only ~3.3 deg/(kcal/mol) within the considered 6 kcal/mol limit. Another planar molecule, oxanthrene, was also considered: While formally antiaromatic, it adopts a planar conformation in the solid state.<sup>3</sup> Interestingly, oxanthrene (Figure 7, scaffold B) is substantially more flexible than anthracene, exhibiting deviations from planarity of 7.8 deg/(kcal/mol) within the 6 kcal/mol limit. The final "planar" molecule considered was 9,9-dimethylxanthene (Figure 7, scaffold E). In the initial comparison to oxanthrene, it appears only marginally more flexible, indicating a flexibility index of 9.5 deg/(kcal/mol) within the 6 kcal/mol limit. However, the PES of 9,9-dimethylxanthene also reveals a very shallow surface between the dihedral angles of roughly 140-220°; remarkably, within this range of angles, 9,9dimethylxanthene is virtually barrierless with a remarkably high flexibility index of 70.3 deg/(kcal/mol).

Next, scaffolds that are inherently folded in their ground state structures were considered. Thianthrene (Figure 7, scaffold C) and 1 (Figure 7, scaffold D) exhibited similar energy profiles, with the inversion barrier of thianthrene being roughly 1.5 kcal/mol less than that of 1. Thianthrene deviates from the folded to planar conformation with a flexibility index of 10.6 °C/(kcal/mol), while 1 provided a slightly less dynamic index of 8.8 deg/(kcal/mol). Considered holistically,

these data suggest that thianthrene is marginally more flexible than 1. The final molecule considered was mixed chalcogen scaffold phenoxathiin (Figure 7, scaffold F). Its inversion barrier was remarkably lower than that of either thianthrene or 1, being essentially negligible at only 0.61 kcal/mol. This is in line with previous studies that have determined experimentally<sup>36</sup> and theoretically<sup>37</sup> inversion barriers in the range of about 1.2–2.5 kcal/mol. Thus, its characteristic flexibility index of deviation from the inherently folded to planar conformation results in a flexibility index of 51.1 deg/(kcal/mol). This suggests that phenoxathiin is considerably more flexible than either thianthrene or 1, although its movement is somewhat more constricted, processing rather freely from only 150 to 210° while thianthrene and 1 exhibit movement through a larger range, from approximately 125–235°.

## 3. CONCLUSIONS

In summary, we generated improved synthetic procedures and full characterization (1H, 13C, and 77Se NMR and single-crystal X-ray structures) for 1, 2, trans-3 and the previously unknown selenanthrene-dioxide 4. The single-crystal X-ray structures of 1, 2, trans-3 and 4 demonstrated a strong dependence of the fold angle on the total number of oxygen atoms, a trend absent in the sulfur-containing analogues. Variable-temperature <sup>1</sup>H NMR provided insights into the conformational equilibria of 2 and 4 and enabled the calculation of a barrier for ring inversion for trans-3. Correlated DFT calculations enabled the estimation of inversion barriers for 1, 2, trans-3 and 4. It was found that, upon comparison to the sulfur analogues, compounds 1, 2, trans-3 and 4 possess slightly larger barriers for ring inversion. This is attributable to (i) more bond-angle strain in the transition state and (ii) enhanced intramolecular interactions originating from the highly polar seleniumoxygen bonds present in 2, trans-3 and 4. Lastly, a comparison of the PES of 1 against those of other tricyclic molecules was performed by using DFT calculations.

Importantly, we propose that moving forward, the extent of flexibility and dynamic motion in compounds, such as the tricyclic scaffolds discussed herein, be characterized by the "energetic flexibility index" in units of  $\deg/(kcal/mol)$  within a sensible energetic limit, such as  $\sim 5$  to 6 kcal/mol as used in this study. It is intended that researchers can utilize this quantitative indicator as both an analytical tool to understand reactivity properties and a design tool for the generation of rational hypotheses regarding the influence of dynamic motion on reactivity at metal centers.

# 4. EXPERIMENTAL SECTION

**4.1. General Procedures.** Unless otherwise noted, all reactions were performed in a fume hood under a N2 atmosphere using standard Schlenk techniques. All glassware was dried in a 110 °C oven for at least 16 h before use. DMSO was vacuum-distilled from CaH<sub>2</sub> and stored over 4 Å molecular sieves. All other reaction solvents were dried by using a Pure Process Technology solvent purification system equipped with activated alumina columns. Solvents used for extraction or chromatography were obtained from Fisher Scientific and used without further purification. The oxidant m-CPBA was purchased from Sigma-Aldrich stabilized on benzoic acid (25% w/w) and was purified according to the literature procedure.<sup>38</sup> The reagent 1,2-diiodobenzene was purchased from Oakwood Chemical and used as received. Selenium powder and copper salts were purchased from Strem and used as received. All other organic reagents were purchased from either TCI Chemical or Sigma-Aldrich and used as received. All other inorganic reagents were purchased from Fisher Scientific and used as received. <sup>1</sup>H, <sup>13</sup>C (101 MHz) and <sup>77</sup>Se NMR (76 MHz) spectra were collected on a Varian DirecDrive instrument equipped with a 400 MHz OneNMR 5 mm probe. Variable temperature NMR spectra were collected on a Varian Oxford 600 MHz instrument equipped with a 600 MHz OneNMR 5 mm probe. Chemical shifts for  $^{1} ext{H}$  and  $^{13} ext{C}$  are reported in ppm  $(\delta)$  and calibrated using residual nondeuterated solvent peaks as internal references. Chemical shifts for <sup>77</sup>Se spectra are reported in parts per million ( $\delta$ ) and referenced externally to dimethyl selenide.

**Caution!** Dimethyl selenide is volatile and acutely toxic. Extreme care must be used when working with this reagent and adequate safety precautions in place to prevent inhalation or direct contact with skin.

4.1.1. Optimization Experiments for the Synthesis of Selenanthrene (1). To an oven-dried 10 mL Schlenk flask was added the
specified amounts of gray selenium powder (1 or 1.5 equiv), copper
salt (0.1 equiv), alkali carbonate (2 equiv), and 1,10-phenanthroline
(0.2 equiv) (see Table 1 for all screened conditions). The flask was
then sealed with a septum and inerted using 3× vacuum/N<sub>2</sub> cycles.
Next, 2 mL of anhydrous DMSO was injected using a syringe,
followed by 1,2-diiodobenzene (1 mmol). The mixture was heated at
the specified temperature for the specified time. After cooling, a 0.2
mL aliquot was extracted with 2 mL DCM and washed with DI water
(2 mL, 5×). The organic layer was isolated and dried over sodium
sulfate and the volatiles were removed. The mixture was then assayed
using <sup>1</sup>H NMR spectroscopy (CDCl<sub>3</sub>) to determine the ratio of the
starting material (1,2-diiodobenzene) to 1.

4.1.2. Selenanthrene (1). A mixture of 1,2-diiodobenzene (1.96 mL, 15 mmol, 1.0 equiv), selenium powder (1.776 g, 22.5 mmol, 1.5 equiv), cupric acetate (0.2994 g, 1.5 mmol, 0.1 equiv), potassium carbonate (4.146 g, 30 mmol, 2 equiv), and 1,10-phenanthroline (0.540 g, 3 mmol, 0.2 equiv) was dissolved in anhydrous DMSO (30 mL) under a N2 atmosphere. The solution was heated to 100 °C in an oil bath and stirred for 72 h. After cooling, dichloromethane (100 mL) was added, and the solution was washed with deionized water (5× 50 mL). The organic phase was dried over sodium sulfate, and the solvent was removed with rotary evaporation to afford a yellow powder. The powder was purified with flash chromatography using isocratic hexanes, resulting in 1 as an off-white microcrystalline powder (2.040 g, 87%). <sup>1</sup>H NMR (600 MHz, CD<sub>2</sub>Cl<sub>2</sub>): δ 7.72 (ddd, J = 5.8, 3.4, 0.6 Hz, 1H), 7.29-7.24 (m, 1H). <sup>13</sup>C NMR (101 MHz, CDCl<sub>3</sub>)  $\delta$ : 134.64, 131.36, 128.22. <sup>77</sup>Se NMR (76 MHz, CDCl<sub>3</sub>):  $\delta$ 466.83.

4.1.3. Selenanthrene 5-Oxide (2). Selenanthrene (1) (1.00 g, 3.22 mmol, 1.0 equiv) and m-CPBA (0.8335 g, 4.83 mmol, 1.5 equiv) were dissolved in DCM (40 mL) and the solution was stirred at 0 °C for 2 h using an ice bath. The reaction was quenched with sodium carbonate (0.513 g, 4.83 mmol) and potassium sulfite (0.610 g, 4.83 mmol) dissolved together in water (40 mL). The organic phase was washed with water (2× 40 mL), and then the aqueous layer was extracted with ethyl acetate (3× 40 mL). The combined organic phases were dried over sodium sulfate and then evaporated. The resulting solid was purified via column chromatography in isocratic DCM to afford 2 as a white powder (0.461 g, 44%). <sup>1</sup>H NMR (600 MHz, CD<sub>2</sub>Cl<sub>2</sub>)  $\delta$ : 7.91 (dd, J = 7.8, 1.4 Hz, 1H), 7.82 (dd, J = 7.6, 1.2 Hz, 1H), 7.57 (td, J = 7.6, 1.2 Hz, 1H), 7.43 (td, J = 7.5, 1.4 Hz, 1H). <sup>13</sup>C NMR (101 MHz, CDCl<sub>3</sub>)  $\delta$ : 143.96, 132.32, 130.66, 129.30, 127.10, 126.88. <sup>77</sup>Se NMR (76 MHz, CD<sub>2</sub>Cl<sub>2</sub>):  $\delta$  852.71, 389.03.

Article

4.1.4. Selenanthrene 5,10-Dioxide (trans-3). Selenanthrene (1) (0.300 g, 0.96 mmol, 1.0 equiv) and m-CPBA (0.497 g, 2.88 mmol, 3.0 equiv) were dissolved in DCM (30 mL), and the solution was stirred under reflux for 24 h. The reaction was quenched with 1 M aqueous sodium carbonate (30 mL) and extracted with water (2× 30 mL), and then the aqueous was washed with diethyl ether (3 × 30 mL). The aqueous phase was extracted with 15% isopropanol/DCM (3× 15 mL), and the organic layer was then dried over sodium sulfate and evaporated to afford trans-3 as a white powder (0.0847 g, 26%). <sup>1</sup>H NMR (600 MHz, CDCl<sub>3</sub>, -60 °C):  $\delta$  8.26 (d, J = 7.7 Hz, 1H), 7.95-7.90 (m, 1H), 7.72-7.66 (m, 1H), 7.60-7.52 (m, 1H). Suitable  $^{13}$ C and  $^{77}$ Se NMR spectra of trans-3 could not be obtained due to the significant broadening of resonances caused by the dynamic ring inversion process.

4.1.5. Selenanthrene 5,5,10-Trioxide (4). Selenanthrene (1) (0.300 g, 0.96 mmol, 1.0 equiv) and m-CPBA (0.663 g, 3.84 mmol, 4.0 equiv) were dissolved in DCM (30 mL), and then the solution was stirred while refluxing for 48 h. The reaction was quenched with 1 M aqueous sodium carbonate (30 mL) and extracted with water (2×30 mL), and then the aqueous layer was washed with diethyl ether (3×30 mL). The aqueous phase was extracted with a 15% isopropanol/DCM solution (3×15 mL), and the organic layer was then dried over sodium sulfate and evaporated to afford 4 as a white powder (0.164 g, 48%).  $^{1}$ H NMR (600 MHz, DMSO- $^{2}$ 6):  $\delta$  8.15 (dd,  $^{1}$  = 7.6, 1.3 Hz, 2H), 7.96 (td,  $^{1}$  = 7.6, 1.3 Hz, 1H), 7.87 (td,  $^{1}$  = 7.6, 1.3 Hz, 1H).  $^{13}$ C NMR (101 MHz, CDCl<sub>3</sub>)  $\delta$ : 145.60, 138.16, 134.63, 132.23, 128.23, 126.83.  $^{77}$ Se NMR (76 MHz, DMSO- $^{4}$ 6)  $\delta$ : 934.28, 866.97.

4.2. Computational Methods. All calculations were performed using the ORCA 5.0 software package.<sup>39</sup> Output files from ORCA calculations were manipulated in either the Chemcraft<sup>40</sup> or Mercury<sup>41</sup> software packages. Initial ground state and transition state calculations for 1, 2, trans-3 and 4 were performed at the BP86/def2-SVP and OPBE/ZORA-def2-TZVP levels of theory. In both cases, atompairwise dispersion corrections to the DFT energy with Becke-Johnson damping were applied, and SCF convergence tolerances were set to  $1.0 \times 10^{-8}$  au. Crystal structure coordinates were used as initial structure guesses. For the OPBE/ZORA-def2-TZVP calculations, relativistic corrections were applied using ZORA<sup>42</sup> as it is implemented in ORCA, and the solvation model based on density (SMD)<sup>43</sup> was used to implicitly model solvation. In each case, chloroform was chosen as the implicit solvent. Analytical frequency calculations were performed to confirm the correct identification of ground state minima and transition state maxima (saddle points). For ground state frequency calculations, it was verified that the output contained no zero and no imaginary frequencies. Transition state calculations were verified by confirming that a single imaginary frequency was obtained. It is important to note that the SMD implicit solvation model could not be used for the analytical frequency calculations as the analytical Hessian has not been implemented for SMD in ORCA. Thus, the ground state and transition state structures at the OPBE/ZORA-def2-TZVP level of theory that include the SMD solvation model could not be verified by frequency analysis.

Next, PES scans of 1, 2, trans-3 and 4 were performed first at the BP86/def2-SVP and then at the OPBE/ZORA-def2-TZVP levels of

theory using the same assumptions, corrections and tolerances as listed above. The structures obtained from the BP86/def2-SVP calculations were used as initial structure guesses for the OPBE/ZORA-def2-TZVP relaxed PES scan calculations. To scan the PES along the "butterfly" motion of the molecules, the dihedral angles were modulated between atoms 1, 2, 5 and 6; and the dihedral angles between atoms 3, 2, 5 and 4 (Figure 8) were constrained to be equal

Figure 8. Numbering scheme for the assignment of dihedral angles, which were constrained during relaxed PES scans.

and allowed to vary (symmetrically) over 32 scans. Molecules that are symmetric with respect to ring inversion (1 and trans-3) required only 16 scans up to dihedral angles of 180° because their energy profiles are by definition symmetric. Analogous PES scan calculations were performed on the molecules listed in Figure 7A–F (anthracene, oxanthrene, thianthrene, 1, 9,9-dimethylxanthene, and phenoxathiin) at the BP86/def2-SVP level of theory using the same assumptions, corrections, and tolerances as listed above.

Initially, the BP86 functional and def2-SVP basis set were selected as they are computationally inexpensive. For calculations at higher levels of theory, the OPBE functional was selected as a benchmark study of diaryl dichalcogenides identified OPBE as a suitable for handling Se and Te containing arenes. <sup>44</sup> The relativistic ZORA-def2-TZVP basis set was selected both to account for the heavy selenium atom and to provide good convergence for geometry optimizations and energy calculations.

## ASSOCIATED CONTENT

# **Solution** Supporting Information

The Supporting Information is available free of charge at https://pubs.acs.org/doi/10.1021/acs.inorgchem.4c00658.

NMR spectra, X-ray crystallographic details, ORTEP diagrams, computational details, PES scans, comparison of computed and experimentally determined bonding metrics, crystal structures of 1, 2, trans-3, 4 and 1,2-bis(4-bromophenyl)diselane (PDF)

## **Accession Codes**

CCDC 2322586–2322590 contain the supplementary crystallographic data for this paper. These data can be obtained free of charge via <a href="www.ccdc.cam.ac.uk/data\_request/cif">www.ccdc.cam.ac.uk/data\_request/cif</a>, or by emailing <a href="mailto:data\_request@ccdc.cam.ac.uk">data\_request@ccdc.cam.ac.uk</a>, or by contacting The Cambridge Crystallographic Data Centre, 12 Union Road, Cambridge CB2 1EZ, UK; fax: +44 1223 336033.

# AUTHOR INFORMATION

# **Corresponding Author**

Michael J. Rose — Department of Chemistry, University of Texas at Austin, Austin, Texas 78712, United States; orcid.org/0000-0002-6960-6639; Email: mrose@cm.utexas.edu

### **Authors**

Alec T. Larson – Department of Chemistry, University of Texas at Austin, Austin, Texas 78712, United States; orcid.org/0009-0000-5975-0023

Brett Boyle — Department of Chemistry, University of Texas at Austin, Austin, Texas 78712, United States; ⊙ orcid.org/0009-0002-4682-7890

Jordan Labrecque — Department of Chemistry, University of Texas at Austin, Austin, Texas 78712, United States;
orcid.org/0000-0003-1744-1489

Anh Ly – Department of Chemistry, University of Texas at Austin, Austin, Texas 78712, United States; orcid.org/0000-0002-8974-9637

Cecilia Bui – Department of Chemistry, University of Texas at Austin, Austin, Texas 78712, United States

Serhii Vasylevskyi — Department of Chemistry, University of Texas at Austin, Austin, Texas 78712, United States;
orcid.org/0000-0001-6219-6051

Complete contact information is available at: https://pubs.acs.org/10.1021/acs.inorgchem.4c00658

### **Notes**

The authors declare no competing financial interest.

### ACKNOWLEDGMENTS

The authors thank Dr. Garrett Blake and Dr. Scott Smith at the University of Texas at Austin NMR Facility for their assistance with the collection of variable-temperature and heteronuclear NMR spectra. We also acknowledge Daniel McIntosh for technical assistance in DFT calculations. The authors are grateful for funding from the National Science Foundation (NSF-CHE 2109175) and the Robert A. Welch foundation (F-1822).

## REFERENCES

- (1) Krafft, F.; Kaschau, A. Ueber Thianthren Und Selenanthren, C<sub>12</sub>H<sub>8</sub>Se<sub>2</sub>. II. Ber. Dtsch. Chem. Ges. **1896**, 29 (1), 443–445.
- (2) Yang, Z.; Fu, Z.; Liu, H.; Wu, M.; Li, N.; Wang, K.; Zhang, S.-T.; Zou, B.; Yang, B. Pressure-Induced Room-Temperature Phosphorescence Enhancement Based on Purely Organic Molecules with a Folded Geometry. *Chem. Sci.* **2023**, *14* (10), 2640–2645.
- (3) Adam, W.; Haas, W.; Sieker, G. Thianthrene 5-Oxide as Mechanistic Probe in Oxygen-Transfer Reactions: The Case of Carbonyl Oxides vs. Dioxiranes. *J. Am. Chem. Soc.* **1984**, *106* (17), 5020–5022.
- (4) Adam, W.; Haas, W.; Lohray, B. B. Thianthrene 5-Oxide as a Mechanistic Probe for Assessing the Electronic Character of Oxygen-Transfer Agents. *J. Am. Chem. Soc.* **1991**, *113* (16), 6202–6208.
- (5) Deubel, D. V. Thianthrene 5-Oxide as a Probe for the Electronic Character of Oxygen-Transfer Reactions: Re-Interpretation of Experiments Required. *J. Org. Chem.* **2001**, *66* (8), 2686–2691.
- (6) Kim, S.; Kwon, Y.; Lee, J.-P.; Choi, S.-Y.; Choo, J. A Theoretical Investigation into the Conformational Changes of Dibenzo-p-Dioxin, Thianthrene, and Selenanthrene. *J. Mol. Struct.* **2003**, *655* (3), 451–458.
- (7) González-Núñez, M. E.; Mello, R.; Royo, J.; Asensio, G.; Monzó, I.; Tomás, F.; López, J. G.; Ortiz, F. L. Conformational Mobility of Thianthrene-5-Oxide. *J. Org. Chem.* **2005**, *70* (9), 3450–3457.
- (8) Chickos, J.; Mislow, K. Conformational Flexibility of Thianthrene and Its Oxides. *J. Am. Chem. Soc.* **1967**, 89 (18), 4815–4816.
- (9) Casarini, D.; Coluccini, C.; Lunazzi, L.; Mazzanti, A. Ring Inversion Dynamics of Derivatives of Thianthrene Di- and Tetraoxide. *J. Org. Chem.* **2006**, *71* (16), 6248–6250.
- (10) Labrecque, J.; Cho, Y.-I.; McIntosh, D. K.; Agboola, F.; Rose, M. J. Distal Scaffold Flexibility Accelerates Ligand Substitution Kinetics in Manganese(I) Tricarbonyls: Flexible Thianthrene versus Rigid Anthracene Scaffolds. *Dalton Trans.* **2023**, *52* (13), 4028–4037.
- (11) Sato, R. Product Class 6:1,4-Diselenins. In *Hetarenes and Related Ring Systems*; Science of Synthesis; Georg Thieme Verlag KG: Stuttgart, 2015; Category 2, Vol. 16.
- (12) Prasad, C. D.; Balkrishna, S. J.; Kumar, A.; Bhakuni, B. S.; Shrimali, K.; Biswas, S.; Kumar, S. Transition-Metal-Free Synthesis of

- Unsymmetrical Diaryl Chalcogenides from Arenes and Diaryl Dichalcogenides. J. Org. Chem. 2013, 78 (4), 1434–1443.
- (13) Wan, J.; Liu, Y.; Zhang, Y. Sample method for synthesis of thianthrene based on sulfur powder. CN 104844565 A, 2015.
- (14) Lv, W.; Song, Y.; Lv, X.; Yuan, J.; Zhu, K. Synthesis, Structure, and Host-Guest Chemistry of a Pair of Isomeric Selenanthrene-Bridged Molecular Cages. *Chin. Chem. Lett.* **2023**, 34 (11), 108179.
- (15) DiMucci, I. M.; Lukens, J. T.; Chatterjee, S.; Carsch, K. M.; Titus, C. J.; Lee, S. J.; Nordlund, D.; Betley, T. A.; MacMillan, S. N.; Lancaster, K. M. The Myth of D<sup>8</sup> Copper(III). *J. Am. Chem. Soc.* **2019**, *141* (46), 18508–18520.
- (16) Jiang, Y.; Qin, Y.; Xie, S.; Zhang, X.; Dong, J.; Ma, D. A General and Efficient Approach to Aryl Thiols: CuI-Catalyzed Coupling of Aryl Iodides with Sulfur and Subsequent Reduction. *Org. Lett.* **2009**, 11 (22), 5250–5253.
- (17) Tartar, H. V.; Draves, C. Z. Reaction of Sulfur with Alkali and Alkaline Earth Hydroxides in Aqueous Solutions. *J. Am. Chem. Soc.* **1924**, *46* (3), 574–581.
- (18) Eggert, H.; Nielsen, O.; Henriksen, L. Selenium-77 NMR. Application of  $J_{\text{Se-Se}}$  to the Analysis of Dialkyl Polyselenides. *J. Am. Chem. Soc.* **1986**, *108* (8), 1725–1730.
- (19) Beletskaya, I. P.; Sigeev, A. S.; Peregudov, A. S.; Petrovskii, P. V.; Khrustalev, V. N. Microwave-Assisted Synthesis of Diaryl Selenides. Elucidation of Cu(I)-Catalyzed Reaction Mechanism. *Chem. Lett.* **2010**, 39, 720–722.
- (20) Furukawa, N.; Kimura, T.; Ishikaa, Y.; Minoshima, Y. First Preparation, Structural Determination by X-Ray Crystallographic Analysis and MO-Calculations of Dibenzo[Bc,Fg] [1,4]-Dithiapentalene and Its Selenium Analogs. *Heterocycles* 1994, 37 (1), 541.
- (21) Cullinane, N. M. Some Derivatives of Selenanthren. J. Chem. Soc. 1951, 237.
- (22) Bergson, G.; Lindstedt, S.; Norman, A.; Schliack, J.; Reio, L. A New Synthesis of Selenanthren-5,10-Dioxide. *Acta Chem. Scand.* **1957**, *11*, 580–581.
- (23) Kamigata, N. Synthesis and Stereochemistry of Chiral Selenoxides and Telluroxides. *Phosphorus, Sulfur, Silicon Relat. Elem.* **2001**, 171 (1), 207–229.
- (24) Adam, W.; Curci, R.; Edwards, J. O. Dioxiranes: A New Class of Powerful Oxidants. Acc. Chem. Res. 1989, 22 (6), 205–211.
- (25) Wood, R. G.; Williams, G. Folding of the Selenanthren Molecule. *Nature* **1942**, *150* (3802), 321–322.
- (26) Meyers, E. A.; Irgolic, K. J.; Zingaro, R. A.; Junk, T.; Chakravorty, R.; Dereu, N. L. M.; French, K.; Pappalardo, G. C. The Crystal Structures of 9,10-Dichalcogenaanthracenes,  $C_{12}H_8XY$ , (X,Y) = (S, Se), (S, Te), (Se, Te), and (O, Se). Phosphorus Sulfur Relat. Elem. 1988, 38 (3–4), 257–269.
- (27) Farrugia, L. J. WinGX and ORTEP for Windows: An Update. J. Appl. Crystallogr. 2012, 45 (4), 849–854.
- (28) Tripathi, A.; Deka, R.; Butcher, R. J.; Turner, D. R.; Deacon, G. B.; Singh, H. B. Exploring the Reactivity of L-Tellurocystine, Te-Protected Tellurocysteine Conjugates and Diorganodiselenides towards Hydrogen Peroxide: Synthesis and Molecular Structure Analysis. New J. Chem. 2022, 46 (22), 10550–10559.
- (29) Zak, Z.; Keznikl, L. Crystal Structure of Diphenylselenon, (C<sub>6</sub>H<sub>5</sub>)<sub>2</sub>SeO<sub>2</sub>. Z. Kristallogr. Cryst. Mater. **1995**, 210 (4), 302.
- (30) Eccles, K. S.; Morrison, R. E.; Stokes, S. P.; O'Mahony, G. E.; Hayes, J. A.; Kelly, D. M.; O'Boyle, N. M.; Fábián, L.; Moynihan, H. A.; Maguire, A. R.; Lawrence, S. E. Utilizing Sulfoxide···Iodine Halogen Bonding for Cocrystallization. *Cryst. Growth Des.* **2012**, *12* (6), 2969–2977.
- (31) Cai, X.; Qiao, Z.; Li, M.; Wu, X.; He, Y.; Jiang, X.; Cao, Y.; Su, S.-J. Purely Organic Crystals Exhibit Bright Thermally Activated Delayed Fluorescence. *Angew. Chem., Int. Ed.* **2019**, 58 (38), 13522–13531
- (32) Wen, Y.; Liu, H.; Zhang, S.-T.; Pan, G.; Yang, Z.; Lu, T.; Li, B.; Cao, J.; Yang, B. Modulating Room Temperature Phosphorescence by Oxidation of Thianthrene to Achieve Pure Organic Single-Molecule White-Light Emission. *CCS Chem.* **2021**, *3* (7), 1940–1948.

(33) Crews, P.; Rodríguez, J.; Jaspars, M. Organic Structure Analysis, 1st ed.; Oxford University Press, Inc., 1998; pp 111–128.

Article

- (34) Singh, P.; McKinney, J. D. Dibenzo-p-Dioxin: A Refinement. Acta Crystallogr., Sect. B: Struct. Crystallogr. Cryst. Chem. 1978, 34 (9), 2956–2957.
- (35) Dereu, N. L. M.; Zingaro, R. A.; Meyers, E. A. Telluranthrene, C<sub>12</sub>H<sub>8</sub>Te<sub>2</sub>. Cryst. Struct. Commun. **1981**, 10, 1359.
- (36) Davies, M.; Swain, J. Dielectric Studies of Configurational Changes in Cyclohexane and Thianthrene Structures. *Trans. Faraday Soc.* 1971, 67 (0), 1637–1653.
- (37) Gad El-karim, I. A. Quantum Mechanical Study of Substituted Phenoxathiin: A Study of the Structure of Fluorinated Phenoxathiins. *J. Mol. Struct.* **2010**, 945 (1–3), 17–22.
- (38) Horn, A.; Kazmaier, U. Purified mCPBA, a Useful Reagent for the Oxidation of Aldehydes. Eur. J. Org Chem. 2018, 2018 (20–21), 2531–2536
- (39) Neese, F. Software Update: The ORCA Program System—Version 5.0. Wiley Interdiscip. Rev.: Comput. Mol. Sci. 2022, 12 (5), No. e1606.
- (40) Chemcraft-Graphical Software for Visualization of Quantum Chemistry Computations. Version 1.8, Build 682. https://www.chemcraftprog.com (accessed Jan 22, 2024).
- (41) Macrae, C. F.; Sovago, I.; Cottrell, S. J.; Galek, P. T. A.; McCabe, P.; Pidcock, E.; Platings, M.; Shields, G. P.; Stevens, J. S.; Towler, M.; Wood, P. A. Mercury 4.0: From Visualization to Analysis, Design and Prediction. *J. Appl. Crystallogr.* **2020**, *53* (1), 226–235.
- (42) Lenthe, E. v.; Baerends, E. J.; Snijders, J. G. Relativistic Regular Two-Component Hamiltonians. J. Chem. Phys. 1993, 99, 4597–4610.
- (43) Marenich, A. V.; Cramer, C. J.; Truhlar, D. G. Universal Solvation Model Based on Solute Electron Density and on a Continuum Model of the Solvent Defined by the Bulk Dielectric Constant and Atomic Surface Tensions. *J. Phys. Chem. B* **2009**, *113* (18), 6378–6396.
- (44) Zaccaria, F.; Wolters, L. P.; Fonseca Guerra, C.; Orian, L. Insights on Selenium and Tellurium Diaryldichalcogenides: A Benchmark DFT Study. *J. Comput. Chem.* **2016**, *37* (18), 1672–1680.